nature neuroscience

Biophysical mechanisms underlying olfactory receptor neuron dynamics

Katherine I Nagel[1] & Rachel I Wilson[1,2]

The responses of olfactory receptor neurons (ORNs) to odors have complex dynamics. Using genetics and pharmacology, we found that these dynamics in *Drosophila* ORNs could be separated into sequential steps, corresponding to transduction and spike generation. Each of these steps contributed distinct dynamics. Transduction dynamics could be largely explained by a simple kinetic model of ligand-receptor interactions, together with an adaptive feedback mechanism that slows transduction onset. Spiking dynamics were well described by a differentiating linear filter that was stereotyped across odors and cells. Genetic knock-down of sodium channels reshaped this filter, implying that it arises from the regulated balance of intrinsic conductances in ORNs. Complex responses can be understood as a consequence of how the stereotyped spike filter interacts with odor- and receptor-specific transduction dynamics. However, in the presence of rapidly fluctuating natural stimuli, spiking simply increases the speed and sensitivity of encoding.

The fluctuations created by a turbulent odor plume can carry useful information about the chemical environment, and there is evidence that insects use this information to help locate odor sources[1,2]. However, olfactory systems seem to be poorly suited to encode fluctuations, because even simple odor pulses generally elicit prolonged temporal patterns of activity in ORNs. These patterns include epochs of excitation and inhibition, and vary with the type of ORN, odor identity and odor concentration[3–6], often unpredictably. A key question in olfactory coding is how these first-order neurons transform and encode the dynamics of fluctuating stimuli.

Many mechanisms have been proposed to shape the dynamics of ORN responses. These include second-messenger pathways[7,8], neuromodulators[9] and buffering by odorant-binding proteins[10,11]. However, recent discoveries suggest that olfactory transduction in insects may be simpler than previously thought. First, swapping odorant receptors between *Drosophila* ORNs also swaps their odor-evoked temporal patterns[11]. This implies that the differences between these temporal patterns are a property of the receptors themselves. Second, there is evidence that *Drosophila* odorant receptors do not couple to G proteins and instead function as ligand-gated ion channels[12–14]. This argues against a major role for second-messenger pathways in shaping ORN response dynamics, although the issue remains controversial[15]. Third, recent findings suggest that odor-evoked inhibition in *Drosophila* ORNs represents inverse agonism, meaning that the odor stabilizes an inactive state of the receptor[11]. This explains why the same odor can be either excitatory or inhibitory depending on the receptor[6], and why swapping receptors can produce a swap in the polarity of an ORN's response to an odor[11].

In light of these discoveries, we set out to understand the origins of dynamic spike patterns in *Drosophila* ORNs and how these dynamics affect responses to rapid odor fluctuations. We found that these dynamics could be understood in terms of two elementary biophysical processes acting in sequence: transduction and spike generation. Both shaped the dynamics of neural activity, and the interaction between the two could give rise to complex patterns. However, in the presence of rapidly-fluctuating odor plumes, ORN responses were surprisingly simple: transduction acted as an odor- and receptor-specific lowpass filter, whereas spike generation accentuated high-frequency fluctuations that were diminished during transduction.

RESULTS

ORN spiking dynamics are odor and receptor dependent

Odor-evoked spike trains in *Drosophila* ORNs have odor- and receptor-specific dynamics[4,6,16]. In the same ORN, different odors can evoke similar mean firing rates but different temporal patterns of spiking. For example, one odor produced a transient peak at onset and inhibition at offset, whereas another produced only a modest peak at onset and no offset inhibition (**Fig. 1a**,**b**). A single odor could also produce distinct temporal patterns in different neurons: for example, a tonic response in one neuron (**Fig. 1b**) but a phasic response in another (**Fig. 1c**).

We also observed more complex responses. For example, responses could show a transient peak at odor onset, followed by inhibition at odor offset, followed by another period of elevated spiking (**Fig. 1d**). Other odor-receptor combinations produced inhibition during the odor pulse, followed by elevated firing after odor offset (**Fig. 1e**). In this study, we set out to understand the origins of these dynamics and their implications for encoding fluctuating stimuli.

Measuring transduction and spiking in single ORNs

We hypothesized that some aspects of these dynamics reflect transduction events, whereas others reflect events that link transduction to spiking. We therefore set out to obtain independent measures of

[1]Department of Neurobiology, Harvard Medical School, Boston, Massachusetts, USA. [2]Howard Hughes Medical Institute, Harvard Medical School, Boston, Massachusetts, USA. Correspondence should be addressed to R.I.W. (rachel_wilson@hms.harvard.edu).

Received 30 August 2010; accepted 25 November 2010; published online 9 January 2011; doi:10.1038/nn.2725

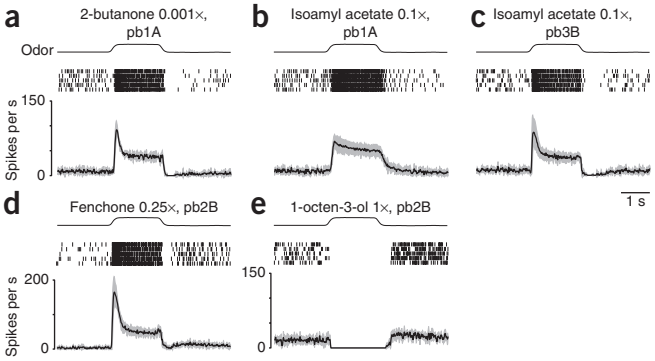

Figure 1 Temporal patterns of ORN spiking are cell and odor dependent. Rasters and peristimulus time histograms (PSTHs; mean ± s.d.) show ORN spiking responses to an odor pulse (1.7 s duration, odors diluted in paraffin oil as labeled). The time course of the odor pulse (top) is not square because it is slightly smoothed by our odor delivery device (**Supplementary Fig. 1**). (**a**) An example of a response with a strong onset transient and offset inhibition. (**b**) In the same type of ORN, a different stimulus drove a similar steady-state firing rate, but the onset transient was weaker and there was no offset inhibition. (**c**) The same stimulus drove a strong onset transient and offset inhibition in a different type of ORN. (**d**) A more complex response, with an onset transient, then offset inhibition, then more excitation. (**e**) An example of inhibition followed by excitation. Each trace represents the mean of 5–6 sensillum recordings, each in a different fly.

transduction and spiking in single ORNs (**Supplementary Fig. 1**). Transduction occurs in the dendrites of ORNs, where odorant receptor proteins are localized[13,17], with one odorant receptor type per cell. ORN dendrites are packaged into finger-like sensilla on the antenna and the maxillary palp. In this study, we focused on the palp, which contains only six types of ORN, arranged as stereotyped pairs in three types of sensilla[4,18] (**Fig. 2a**). Spikes that arise from the two ORNs in a sensillum can be sorted on the basis of their size[4], or by genetically ablating one type of ORN (see Online Methods).

In extracellular recordings from single palp sensilla, odors evoked both a change in spike rate and a deflection in the local field potential (LFP; **Fig. 2b**). The time course of the LFP reflects the time course of the local transmembrane current[19] (see Online Methods) and a downward deflection in the LFP indicates a depolarization of local dendrites[20]. The sensillar LFP is thought to arise mainly from transduction currents[21]. To confirm this, we verified that spikes did not affect LFP dynamics. Injecting the Na^+ channel antagonist tetrodotoxin (TTX, 50 μM) into the palp abolished spiking, but had no effect on LFP time course (**Fig. 2c**). Control injections of saline had no effect. These data are consistent with the idea that the LFP is a proxy for transduction currents, although we cannot exclude a contribution from conductances downstream of transduction but upstream of spiking.

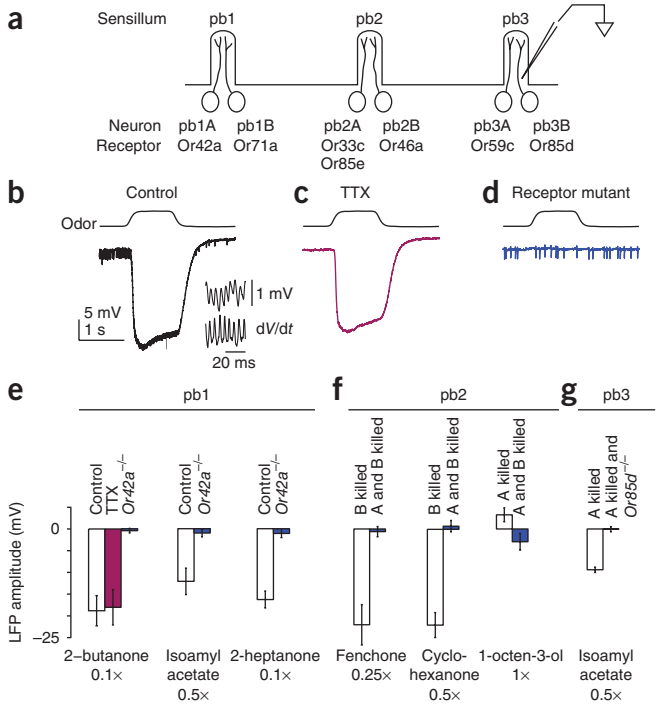

Next, we investigated whether, under certain conditions, the LFP response can be attributed to a single ORN. First, we chose concentrations of specific odors that drive robust responses in a particular type of ORN (pb1A). Then we asked what happened to these responses when the receptor normally expressed by this ORN (OR42a) was mutated. We found that a mutation in Or42a eliminated most pb1 responses to these odors (**Fig. 2d**,**e**), indicating that they were due to this single receptor type. Some of these odors also drove responses in a second sensillum type (pb3) and these responses were unaffected by mutations in Or42a (**Supplementary Fig. 2**). This result indicates that palp sensilla can be electrically isolated from one another, because responses arising from pb3 sensilla are either absent or strongly attenuated in intermingled pb1 sensilla.

Under other conditions, we observed that LFP responses could propagate between nearby sensilla. In particular, LFP responses in antennal sensilla were not well isolated (data not shown), probably because antennal sensilla are packed more densely than palp sensilla. For this study, we recorded only from palp sensilla, and we used genetic ablation of one ORN in a sensillum, or careful choice of odors, to ensure that the LFPs we recorded arose from single ORNs. In each case, we confirmed that the LFP response was largely abolished when the cognate OR was mutated or the cognate ORN was killed genetically (**Fig. 2f**,**g**).

Dynamics of transduction and spike generation

The LFP and spike rate had distinct dynamics (**Fig. 3a**). The LFP time course was similar to the time course of the odor. By contrast,

Figure 2 Field potentials and spikes can be isolated from single ORNs. (**a**) Three types of sensillum in the maxillary palp[4,18]. (**b**) A typical extracellular recording from a pb1 sensillum (stimulus is 2-butanone 0.1×). Enlarged segment at the peak of the response shows individual spikes (inset); taking the first derivative (inset lower trace) facilitates spike detection. (**c**) TTX (50 μM) injected into the palp abolished spikes, leaving the LFP largely unaffected. We fit exponentials to the rising and falling phases of the LFP, and we also computed the overshoot after odor offset; none of these parameters changed significantly (data not shown). (**d**) In *Or42a*$^{-/-}$ flies, this type of sensillum no longer responded to this stimulus, although some spontaneous spikes persisted. (**e**) Mean pb1 LFP responses to selected stimuli were largely unaffected by TTX but were abolished by mutations in *Or42a*. This mutation did not affect responses to these stimuli in a different sensillum type (pb3; **Supplementary Fig. 2**). (**f**) In a pb2 sensillum, responses to fenchone (0.25×) and cyclohexanone (0.5×) were abolished by ablating the A neuron in a genetic background in which B was already ablated. In a background in which A was ablated, 1-octen-3-ol (1×) elicited an inhibitory (upward) LFP that was abolished by killing the B neuron. (The small remaining downward response reflects activity in other sensilla.) (**g**) In pb3 sensilla, LFP responses to isoamyl acetate (0.5×) were abolished by a mutation in *Or85d*. Here the A neuron was ablated genetically. Data in **e**–**g** represent mean ± s.d., $n = 4–7$ recordings each.

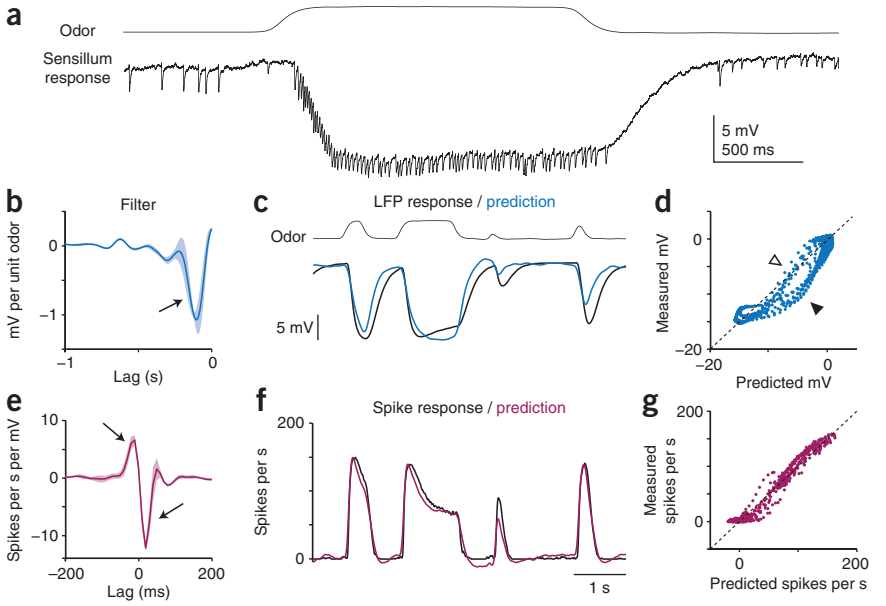

Figure 3 Filter models describe transformations between stimulus, LFP and spikes. (**a**) Time course of odor stimulus and neural response (pb1A; stimulus is 2-butanone 0.01×). Note that the spike rate was highest when the LFP was growing but suppressed when the LFP was recovering. (**b**) Linear filter describing the relationship between the stimulus and the LFP (pb1A, 2-butanone 0.01×; ± s.d.). Arrow indicates single filter lobe. (**c**) The prediction of the filter (blue) was simply an inverted and slightly smoothed version of the odor time course, as expected for a filter with a single lobe. Comparison to the recorded LFP (black, mean of five recordings in five flies) shows that the linear model is an adequate coarse description but underestimates onset rate and overestimates offset rate. (**d**) Actual versus predicted LFP for the stimulus segment shown in **c**. Note that the plot bifurcates because the model underestimated responses during onset (open arrowhead) and overestimated responses during offset (filled arrowhead). (**e**) Linear filter describing the relationship between LFP and spike rate. Arrows indicate two filter lobes. The biphasic filter means that the spike rate increased when the LFP was growing more negative, and was inhibited when the LFP was recovering. Because the negative lobe is larger than the positive lobe, the spike rate remained elevated above baseline during a maintained negative LFP deflection. (**f**) The prediction of the filter (magenta) agrees well with the data (black). (**g**) Actual versus predicted spike rate.

the spike rate was highest when the LFP response was growing and lowest when the LFP was recovering. This implies that the spike rate is sensitive to the slope of the LFP.

To describe these relationships quantitatively, we calculated the linear filters that best summarized each transformation. To calculate the linear filter that related the odor to the LFP, we presented a fluctuating odor waveform while recording the LFP, then cross-correlated the odor waveform with the LFP waveform, and finally corrected for correlations in the odor waveform. Similarly, we also calculated the linear filter that relates the LFP to the spike rate. We did this by cross-correlating the LFP with the spike rate, and then correcting for correlations in the LFP.

The filter that described the transformation from odor to LFP had a single lobe (**Fig. 3b**), indicating that the LFP tended to smooth odor fluctuations. The lobe was negative because odor increases elicited downward deflections in the LFP. The width of this lobe (105 ms half-width in **Fig. 3b**) indicated that the LFP faithfully tracked odor fluctuations up to ~6 Hz (20 dB attenuation). The interval between the lobe and zero indicates the absolute latency of the response, which was less than 10 ms.

To test the filter model, we used it to predict the response to a novel odor waveform (**Fig. 3c**). The prediction was made by convolving the filter with the odor time course. It accurately captured the coarse features of the LFP response (correlation coefficient 0.94 ± 0.006). However, plotting the predicted versus the actual LFP revealed two separate curves (**Fig. 3d**), indicating that LFP onset and offset are asymmetric in a way that cannot be captured by a linear model. We investigate these asymmetries in a later section.

The filter that related the LFP to the spike rate was biphasic (**Fig. 3e**), indicating that the spike rate was sensitive to the LFP slope. The order of the lobes (positive followed by negative) indicated that spiking was promoted by downward deflections in the LFP and inhibited by upward deflections. The slightly larger negative lobe indicated that the spike rate remained above baseline as long as a steady negative LFP deflection persisted. Convolving the spike filter with the LFP produced an excellent prediction of the spike response (correlation coefficient 0.97 ± 0.003; **Fig. 3f**). The spike filter was equally good at predicting responses to fast and slow LFP events, and to short and long odor pulses (data not shown). Plotting the predicted versus actual spike rate revealed a small nonlinearity that is typical of neural responses: the curve flattened near zero because the actual spike rate cannot be negative, and began to saturate at high values (**Fig. 3g**).

We note that this filter has structure to the right of the zero time point, whereas the true filter should not, because spikes are caused by the LFP. This is an artifact of the slow time course of the LFP, which limits how narrow the calculated filter can be (see Online Methods). An idealized filter that is realistically narrow and has no structure to the right of zero can perform as well as the recovered filter, whereas a monophasic filter cannot (**Supplementary Fig. 3**). This implies that the general biphasic shape of the filter is correct, but that its width is over-estimated.

Odor- and cell-dependent transduction and spiking dynamics

We next investigated how the dynamics of these two transformations, transduction and spiking, depend on the odor and the receptor. We recorded LFPs and spikes for several different ligand-receptor combinations. For each combination, we calculated filters that described transduction and spiking.

Filters describing transduction were generally monophasic (**Fig. 4a**), but their width and polarity depended on both the stimulus and the receptor (**Fig. 4**, rows 1–3), corresponding to differences in the speed and polarity of the LFP responses (**Fig. 4b**). Overall, these filters predicted the shape of the LFP well (**Fig. 4b**), implying that transduction could be approximately described as a lowpass filter with a stimulus- and receptor-dependent width and polarity. As in the example above, there were systematic discrepancies at odor onset and offset.

By contrast, filters that described the LFP-to-spiking transformation had a biphasic shape that was relatively similar across stimuli and receptors (**Fig. 4c**). The magnitude of the filter was generally smaller for larger LFP fluctuations, consistent with the idea that neurons adapt to the scale of their inputs[22–24].

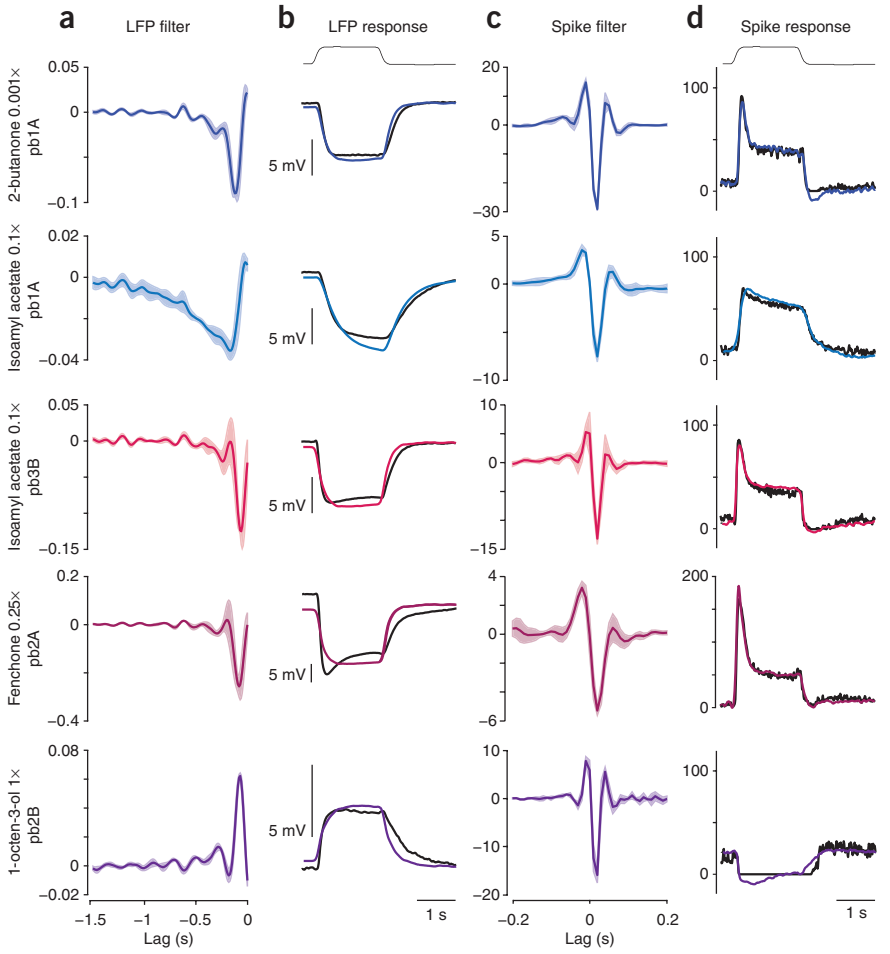

Figure 4 Odor and cell dependence of transduction and spiking dynamics. (**a**) Linear filters describing the relationship between the stimulus and the LFP for five different stimulus-cell combinations. The filter depends on both ligand and receptor. Mean ± s.d. across recordings, $n = 5–6$ each. Units of y axes are mV per unit odor. (**b**) Mean LFP responses for these ligand-receptor combinations (black). Colored lines show the prediction of the linear model, obtained by convolving the corresponding filter in **a** with the stimulus waveform (top). Mean correlation coefficient, 0.93 ± 0.04. (**c**) Linear filters describing the relationship between the LFP and spike rate. These filters have a relatively stereotyped shape, unlike the transduction filters. Units of y axes are spikes per s per mV. (**d**) Mean spiking responses (black) in units of spikes per s. Colored lines show the prediction of the linear model, obtained by convolving the corresponding filter in **c** with the recorded LFP. Mean correlation coefficient, 0.92 ± 0.06.

This filter accurately predicted many details of the spike response (**Fig. 4d**). For example, this filter predicted which responses would show onset transients and offset inhibition (**Fig. 4**, first two rows). It also predicted that when the LFP decayed with multiple slopes (**Supplementary Fig. 4**), there would be distinct phases of inhibited and elevated spiking during odor offset (**Fig. 4**, fourth row). Finally, it predicted elevated spiking after offset of an inhibitory odor (**Fig. 4**, bottom row). The success of this model implies that the transformation of transduction currents into spike rates can be described by a universal biphasic filter.

Genetic manipulation of the differentiating spike filter

What accounts for the biphasic shape of the filter that relates LFP to spike rate? Hodgkin-Huxley models predict that the relationship between input current and spike rate depends on the balance of voltage-dependent Na^+ and K^+ conductances[25]. When the Na^+/K^+ ratio is high, the spike rate reflects a running average of recent input ('integrator' behavior). When this ratio is low, the spike rate responds preferentially to the slope of the input ('differentiator' behavior). To test whether the differentiating shape of the ORN spike filter reflected a specific balance of intrinsic conductances, we asked whether we could reshape the filter by genetically manipulating Na^+ conductances. We chose Na^+ conductances as our target because there is only one Na^+ channel α-subunit in the *Drosophila* genome ($DmNa_v$).

We knocked down $DmNa_v$ in ORNs using transgenic RNA interference (RNAi). This produced a general decrease in spike rate (**Fig. 5a**,**b**) and a change in spike rate dynamics. Specifically, the spiking response became more transient (**Fig. 5c**,**d**). Knockdown of $DmNa_v$ did not affect LFP dynamics, although it slightly reduced LFP magnitude (**Fig. 5e**).

The more transient spiking response suggested that the spike filter had become more differentiating. To examine this directly, we calculated LFP-to-spike filters for a small number of neurons that showed a knockdown phenotype (peak to steady-state firing rate ratio of 1.7–2.3). In these ORNs, the positive and negative lobes of the spike filter were more symmetric—and thus more purely differentiating—than in controls (**Fig. 5f**), whereas the filter that described transduction was not significantly altered (**Fig. 5g**). Together these data suggest that the differentiating spike transformation in ORNs was specified by the regulated expression of voltage-dependent channels in these cells.

A kinetic model can explain asymmetry in transduction

We observed that linear filters approximately described the time course of transduction. However, filter predictions consistently underestimated the speed of transduction onset and overestimated the speed of offset (**Figs. 3c** and **4b**). This is because transduction onset was always faster than offset. A filter, having a single time scale, predicts an average of these two rates.

One model that can account for both of these phenomena is a kinetic model of ligand-receptor interactions. In the simplest case, the level of transduction current is related to the number of activated receptors (OR*), described by

$$R \overset{O}{\longleftrightarrow} OR \longleftrightarrow OR^*$$

where O is the ligand, R is the receptor and R* is the activated receptor. This model accounts for odor-specific transduction rates because the binding and activation constants depend on the identity of both the receptor and the ligand. This model also accounts for the asymmetry we observed between onset and offset rates, because the forward reaction rate depends on the concentration

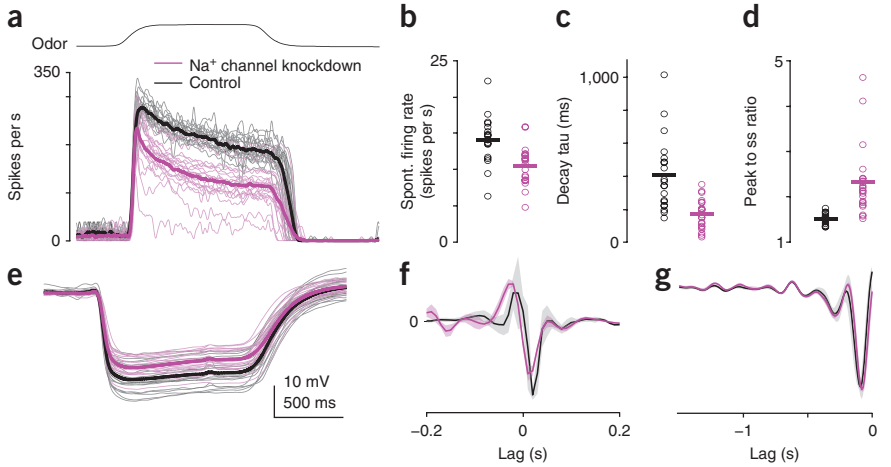

Figure 5 Knocking down $DmNa_v$ makes the LFP-to-spiking transformation more differentiating. (**a**) Firing rates in ORNs with reduced expression of voltage-dependent Na^+ channels (pb1A, stimulus is 2-butanone 0.1×). Thin lines are trial-averaged responses from different recordings ($n = 20–22$ sensilla in 10–11 flies of each genotype); thick lines indicate mean. Mean firing rate during the odor was significantly reduced ($P < 0.01$, *t*-test). (**b**) Spontaneous spike rate was also significantly reduced by Na^+ channel knockdown ($P < 0.01$, *t*-test). (**c**) Decay from the peak odor-evoked firing rate was accelerated by Na^+ channel knockdown, measured here by fitting an exponential to the trace from peak to 200 ms after odor offset ($P < 0.01$, *t*-test). (**d**) The ratio of peak to steady-state firing rate was significantly increased by Na^+ channel knockdown ($P < 0.01$, *t*-test). (**e**) Knockdown had no effect on the time course of the LFP response, although the amplitude was slightly reduced. (**f**) Filters describing the LFP-to-spiking transformation (mean ± s.d., $n = 4$). Knockdown produced more symmetrical positive and negative lobes, indicating a more differentiating transformation. (**g**) Filters describing the stimulus-to-LFP transformation were unaffected by Na^+ channel knockdown, as expected.

of odorant available, whereas the reverse reaction rate depends only on the amount of bound receptor.

One prediction of this model is that onset rates should grow with concentration, but offset rates should not. To test this prediction, we recorded LFP responses to several concentrations of two odors. For both odors, we found that the onset rate grew with increasing concentration, whereas the offset rate was much less sensitive to concentration (**Fig. 6a**,**b**). These data imply that some of the nonlinear features of transduction dynamics arise from elementary properties of receptor binding and activation.

Adaptation slows response kinetics

Another prominent nonlinearity in some responses was a slow decrease in LFP amplitude during the odor pulse (adaptation) which was most prevalent when responses were strong (**Fig. 6a**,**b**). Adaptation was often followed by an overshoot after odor offset (**Fig. 6a**; see also **Supplementary Fig. 4**). This type of adaptation persisted in cells treated with TTX (**Fig. 2b**,**c**), and therefore arose upstream of spiking.

To probe the mechanisms that underlie adaptation, we compared the response to two short test pulses before and after a long adapting pulse (**Fig. 6c**). Adaptation reduced the amplitude of the test pulse response. This effect was reduced as the test pulse concentration increased (**Fig. 6c**,**d**). Thus, adaptation produces a rightward shift in the concentration-response function (**Fig. 6e**). Similarly, adaptation reduced the onset rate of the test pulse (**Fig. 6d**,**f**) and this was also mitigated by high test pulse concentrations. This change in onset kinetics suggests that adaptation acts on the activation of transduction, for example by reducing the affinity of the receptor for ligand or making it more difficult to open the transduction channel (see Discussion).

Adaptation is not intrinsic to the receptor

In a simple scenario, adaptation might reflect inactivation of the odorant receptors themselves. If so, then responses mediated by two

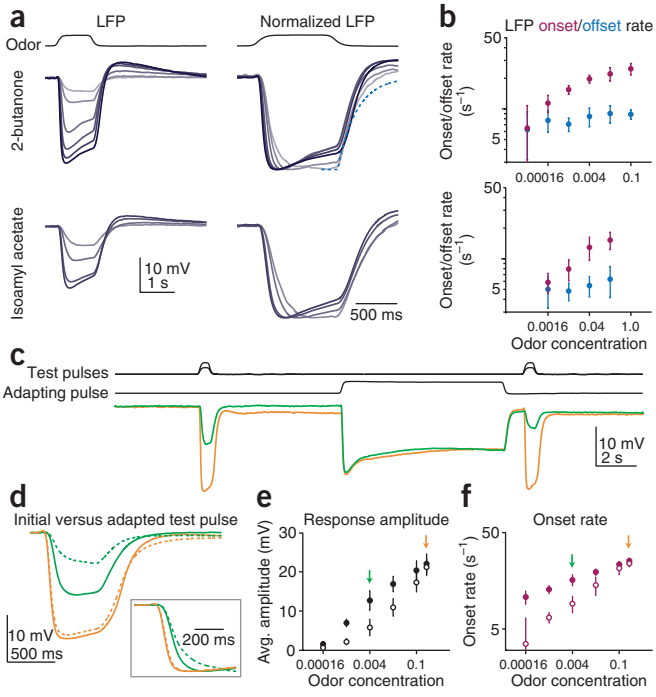

Figure 6 Dynamics of transduction and adaptation. (**a**) LFP recordings from pb1A ORNs illustrate how transduction dynamics depend on odor concentration. Top is 2-butanone (dilutions of 0.1, 0.02, 0.004, 0.0008, 0.00016 and 0.000032×). Bottom is isoamyl acetate (1, 0.2, 0.04, 0.008 and 0.0016×). Traces are means of 5–6 recordings. Traces at right are normalized to the same maximum negative deflection. Dashed blue line shows one exponential fit to response offset; note that only the initial segment was fit and no attempt was made to fit the overshooting later portion. (**b**) On and off rates as a function of odor concentration, mean ± s.d. across recordings. Rates were calculated by fitting exponential curves to the onset and offset phases of the normalized mean LFP. (**c**) A typical recording showing that a long adapting pulse of 2-butanone (0.1×) reduced the amplitude and onset slope of the LFP response to a weak test odor pulse (2-butanone 0.004×, green) but not the response to a strong test odor pulse (2-butanone 0.2×, orange). (**d**) Mean responses to test pulse 1 (solid) and test pulse 2 (dashed) for the two test odors shown in **c**; $n = 6$ recordings. Inset shows the onset phase of these traces normalized to the same amplitude. (**e**) Mean response amplitude (± s.d.) as a function of concentration for test pulse 1 (filled circles) and test pulse 2 (open circles). Arrows indicate the two concentrations shown in **c** and **d**. (**f**) Onset slope as a function of concentration for initial (filled circles) and adapted (open circles) responses.

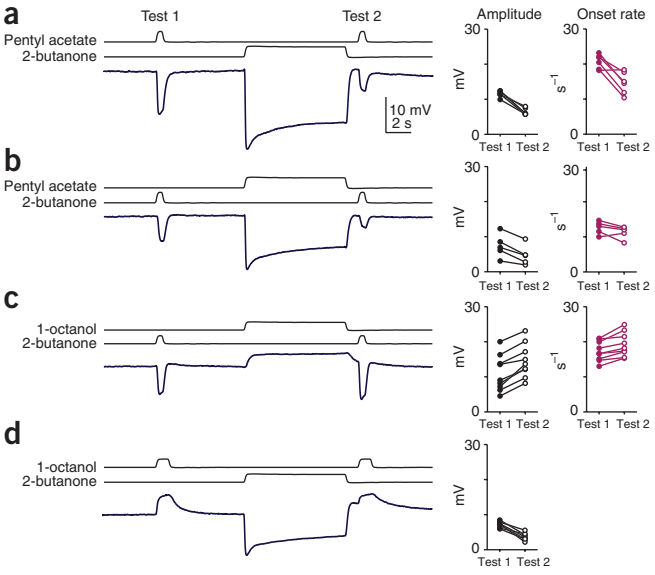

Figure 7 Cross-adaptation between co-expressed odorant receptors. (**a**) A typical recording showing that a long pulse of 2-butanone (0.1×) acting on OR42a adapted the LFP response to a test pulse of another odor (pentyl acetate, 0.02×) acting on OR47a. Group data (right) show that both the amplitude and the onset rate of the second test pulse response were significantly reduced compared to the first test pulse response ($P < 0.01$, $n = 6$, paired t-test). (**b**) Same experiment, but in reverse: a long pulse of pentyl acetate (0.02×) adapted the response to a test pulse of 2-butanone (0.004×). The amplitude of the test pulse response was significantly reduced ($P < 0.01$, $n = 5$, paired t-test). The onset rate was reduced but not significantly ($P = 0.14$, paired t-test). (**c**) A long pulse of 1-octanol (0.1×) acting on OR47b de-adapted the response to a test pulse of 2-butanone (0.1×) acting on OR42a. Both the amplitude and the onset rate of the test pulse response were significantly increased ($P < 0.01$, $n = 9$, paired t-test). (**d**) A long pulse of 2-butanone (0.1×) adapted the response to a test pulse of 1-octanol (0.1×). The amplitude of the test pulse response was significantly reduced ($P < 0.01$, $n = 8$, paired t-test).

receptors in the same ORN should not cross-adapt. To test whether adaptation is intrinsic to the receptor, we ectopically expressed a second receptor (Or47a) in one palp ORN type (pb1A, which natively expresses Or42a). To drive the two receptors independently, we found two stimuli (2-butanone ≤0.1× and pentyl acetate ≤0.02×) that were specific to each receptor (see **Supplementary Fig. 5**).

Next, we asked whether transduction cross-adapts. We found that responses of either receptor type could be adapted by driving the other receptor for a prolonged period (**Fig. 7a**,**b**). Cross-adaptation was similar to self-adaptation, in that adapted responses were smaller and had slower onset rates. Similar to self-adaptation, cross-adaptation could be overcome by using a high test pulse concentration (data not shown). These results imply that self- and cross-adaptation are due to the same phenomenon. Thus, adaptation must involve processes that are shared between receptors, either up- or downstream from the receptor.

Adaptation is induced as a consequence of transduction

If adaptation is initiated by events upstream from ligand binding (for example, if adaptation is caused by depletion of a chaperone that delivers ligand to the receptor) then it should be triggered equally well by odors that inhibit transduction. By contrast, if adaptation is initiated downstream of transduction, then an inhibitory odor should not produce adaptation. To investigate whether adaptation is initiated upstream or downstream of ligand binding, we ectopically expressed a receptor that produces an inhibitory response in pb1A ORNs (OR47b). As before, we used stimuli that act specifically on the native receptor (2-butanone 0.1×) and the ectopic receptor (1-octanol 0.1×; **Supplementary Fig. 5**).

In these ORNs, the inhibitory response did not produce adaptation of the excitatory response. On the contrary, a prolonged inhibitory response seemed to de-adapt the cell: the response to the excitatory test pulse became larger and had a faster onset rate (**Fig. 7c**). This implies that adaptation does not depend merely on odor binding to the receptor. Rather, adaptation depends on transduction. In the same ORNs, the excitatory response reduced the inhibitory response (**Fig. 7d**). (Any effects on onset rate were unclear in this case, because the test pulse coincided with the overshoot produced by the adapting pulse.)

ORNs that ectopically expressed OR47b had significantly higher rates of spontaneous activity than normal ORNs of the same type (36.4 ± 17.9 versus 12.8 ± 2.6 spikes per s; mean ± s.d., $P < 0.01$, t-test, $n = 6$–9; see Online Methods), consistent with a previous report that OR47b confers high spontaneous firing rates when misexpressed[26]. Interestingly, ORNs with the ectopic receptor also had significantly smaller initial responses to 2-butanone (0.1×) (11.0 ± 5.2 versus 20.3 ± 2.5 mV s.d., $P < 0.01$), consistent with the idea that a high basal level of transduction places the cell in a more adapted initial state.

These results further support the idea that adaptation results from either the transduction channel opening or an event downstream. The finding that adaptation alters onset kinetics implies that adaptation targets the pathway that leads to transduction channel opening. Because the target of adaptation is upstream of where adaptation is induced, adaptation likely requires a negative feedback signal.

Responses to natural odor plumes

Our results show that the response dynamics of ORNs arise from the interaction of two dynamic steps, transduction and spike generation. How do natural plumes engage these two distinct steps? To create plumes, we used a fan to produce an air current, and we placed a vial of odor upwind of the fly (**Fig. 8a**). Plumes that reached the fly were monitored using a photoionization detector (PID). Consistent with previous reports[1,2], wind-borne odor signals were intermittent. Odor fluctuations were rapid at high wind speeds and slower at low wind speeds (**Fig. 8a**). When the odor source was displaced laterally, the frequency of odor encounters decreased, and when the source was moved away, encounters became less discrete (**Fig. 8a**). Thus, odor fluctuations provide information about odor source location. Because fluctuations are slowest at low wind speeds, adaptation is likely to be most relevant in this regime.

Consistent with our filter calculations, transduction filtered plumes in a ligand- and receptor-dependent manner. For some ligand-receptor combinations, the LFP faithfully tracked every plume, even at high wind speeds (**Fig. 8b**). For other ligand-receptor combinations, LFP signals were much slower (**Fig. 8c**). To quantify this, we compared the power spectra of these signals. Although the power spectra of plume fluctuations (as reported by the photoionization detector) were similar across ligands, LFP signals were lowpass filtered with a cutoff frequency that depended on the odor-receptor combination (**Fig. 8d**).

To investigate how LFP dynamics depend on LFP amplitude, we identified isolated LFP events, and we binned and averaged these events by amplitude (**Fig. 8e**). This analysis was performed under conditions that increased the incidence of discrete odor encounters (close odor source and high wind speed). We found that the shape of these LFP events was similar for small and large amplitudes, indicating that complex transduction dynamics (like adaptation and overshoot) were not strongly engaged in these conditions. Rather, every plume hit generated an LFP response with similar dynamics.

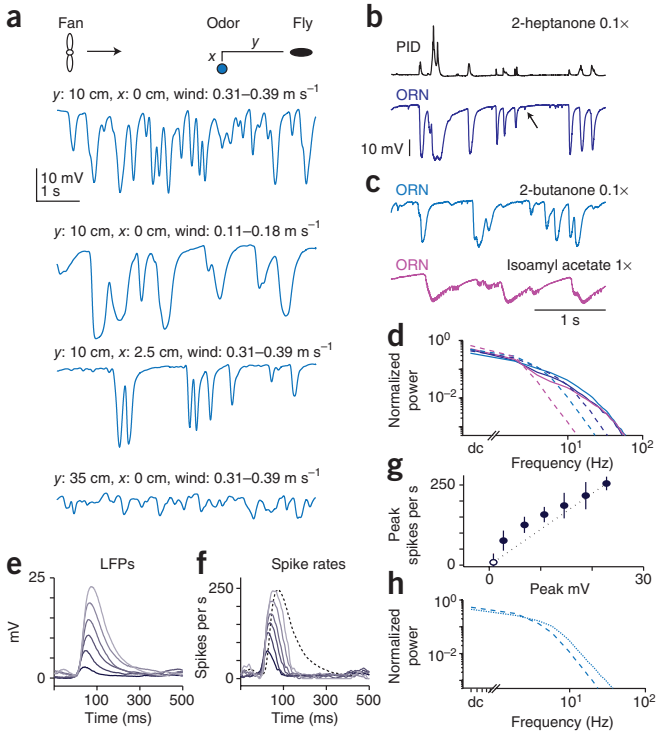

Figure 8 Encoding the dynamics of natural odor plumes. (**a**) Plume dynamics depend on wind speed and odor location. Cartoon schematizes upwind distance (*y*) and crosswind distance (*x*). Traces are LFP recordings from a pb1A ORN responding to 2-butanone (0.1×). (**b**) Simultaneous recordings from a PID and a pb1A ORN (1.5 mm from the PID). Note spontaneous spikes (arrow); odor-evoked spikes are not visible at this scale. (**c**) Responses from the same sensillum in the same configuration with different odors. (**d**) Power spectra of simultaneously measured PID signals (solid lines) and LFP responses (dashed lines). Spectra are normalized to have the same total power. ORN is pb1A, stimuli are color coded as above ($y = 5$ cm, $x = 0$ cm). (**e**) LFP events sorted and averaged by amplitude (inverted here for display). The range of rise times (time from 10% to 90% of peak) was 28–32 ms. Stimulus was 2-butanone 0.1×. Same configuration as in **b** and **c**. (**f**) Average spike rates corresponding to the LFP events in **e**. Dashed trace represents the largest average LFP response, normalized to the same amplitude as the highest average spike rate. (**g**) Peak LFP amplitude versus peak spike rate for the data in **e** and **f**, ± s.e.m. Open symbol, baseline (defined as the 30 ms starting 100 ms before event onset); dashed line, linear extrapolation from this to the largest response. (**h**) Power spectra of LFP (dashed line) and spike rate (dotted line) for responses shown in **c** to 2-butanone 0.1×.

Finally, we investigated how spike generation shapes the response to natural plumes. For each LFP event, we identified the associated spike train and computed the average spike rate associated with each average LFP amplitude. Small LFP events produced disproportionately high spike rates (**Fig. 8f**,**g**), meaning that spike generation tended to emphasize encounters with weak stimuli. The spike response consistently peaked before the LFP response (**Fig. 8f**), indicating that spike generation increased the speed of encoding. Accordingly, we found that the power spectrum of the spike rate contained comparatively more power at high frequencies than the power spectrum of the associated LFP (**Fig. 8h**). Thus, the transformation from transduction to spiking promoted rapid and sensitive encoding of natural stimuli.

DISCUSSION

Input currents and spiking as distinct dynamic processes

Many studies have described the early stages of neural encoding in terms of linear filters, sometimes followed by a static nonlinearity[22,23]. Recently, these techniques have been applied to olfactory systems as well[16,24,27]. The general approach of these studies is to summarize all the dynamic steps between the stimulus and spiking in a single filter.

We used a different approach, motivated by the observation that input currents and spikes have different dynamics. After separating input currents from spiking using genetic and pharmacological tools, we characterized their dynamics independently. We found that transduction was described by an integrating filter. By contrast, spiking was described by a differentiating filter. Thus, transduction smoothes the input signal, whereas spike generation differentiates the transduction response, thereby emphasizing some of the high-frequency fluctuations that were diminished during transduction.

Transduction dynamics depend on the odor and receptor

Olfaction differs from vision in that the dynamics of the primary transduction event depend on the quality of the stimulus. A photoreceptor's response depends only on the number of absorbed photons and the state of the cell, not the wavelength of those photons[28]. By contrast, ORN responses depend on both the receptor the neuron expresses and the identity of the ligand. Explaining why this is true required us to move from a linear model to a kinetic model. Because different ligand-receptor combinations involve different rate constants, a kinetic model accounts for the odor- and receptor dependence of transduction rates. Because forward rates increase with odor concentration and reverse rates do not, a kinetic model also correctly predicts that transduction onset, but not offset, depends on odor concentration.

Like ORNs, central neurons in the insect brain also show cell- and odor-dependent dynamics[27,29,30]. In particular, changes in odor concentration affect the on- and offset portions of these responses in different ways[31]. The finding that qualitatively similar dynamics are observed in ORNs[4,6] suggests that these dynamics are partly inherited from the periphery[32]. Our results show that these dynamics arise at the level of transduction and are a necessary consequence of the most basic kinetic features of chemosensory transduction.

Slow transduction dynamics

In response to strong and prolonged stimuli, odor responses adapt and show overshoot after odor offset. Our results show that these slow dynamics originate at the level of transduction, not spiking. Our results also pinpoint where these dynamics arise.

First, we found that adaptation depends on transduction channel opening. Whereas an excitatory odor response increased adaptation, an inhibitory response decreased adaptation. Because the effect of an odor on the adaptation state of a cell depends on how the odor affects transduction, adaptation cannot be induced before transduction.

Second, we found that adapted responses look like unadapted responses to a lower odor concentration. Specifically, onset rates are slowed. This result rules out a mechanism in which adaptation increases the rate of transduction shut-off, because this would produce faster rather than slower kinetics[33]. It also rules out a mechanism in which adaptation targets an intrinsic conductance downstream of transduction, because this would not slow the rate of transduction onset. Finally, adaptation is unlikely to be due to a change in the driving force for transduction currents, because adaptation outlasts the LFP response to the adapting pulse by several seconds. Adaptation is most likely to involve a decrease in ligand binding affinity or a decrease in the efficacy of channel gating, both of which slow onset kinetics.

Third, adaptation probably involves a diffusible factor. Adaptation is induced as a consequence of the opening of transduction channels, but targets the activation of transduction, implying that it involves a negative feedback signal. What might this signal be? Previous studies reported that mutations in either inositol triphosphate receptors or the TRP channel can reduce adaptation in *Drosophila* ORNs[7,34], suggesting that cytoplasmic calcium is involved. Furthermore, odors induce calcium influx in heterologous cells that express *Drosophila* odorant receptors[12]. Resting calcium in these cells is decreased by an extracellular chelator, consistent with our conclusion that transduction and adaptation can occur spontaneously. Thus, calcium is a good candidate for a diffusible adaptation factor.

The transduction channel in *Drosophila* ORNs probably contains the product of the *Or83b* gene, because a mutation in the putative pore domain of Or83b changes the ionic selectivity of the channel[15]. Odorant receptors are thought to form heteromeric complexes with OR83b[12,13,35]. Alternatively, odorant receptors might gate OR83b through a direct but transient association[15]. Our results are broadly consistent with either alternative.

If the receptor forms a stable heteromer with OR83b (**Supplementary Fig. 6**), then adaptation probably involves changes in both affinity and efficacy. A decrease in affinity is necessary to explain the rightward shift in the concentration-response function (**Fig. 6e**), and a decrease in efficacy is necessary to explain the overshoot after odor offset (**Fig. 6a**). Alternatively, if the activated receptor gates OR83b through an additional step (**Supplementary Fig. 6**), both overshoot and the rightward shift can be explained by a decrease in the efficacy of channel gating. In this model, overshoot arises because both spontaneously active receptors (R*) and odor-activated receptors (OR*) have a diminished ability to open the channel. A rightward shift in the concentration-response function occurs so long as the pool of activated receptors can fully activate most of the available transduction channels at high odor concentrations (**Supplementary Fig. 6**).

In mammalian ORNs, adaptation is due to calcium-calmodulin acting as an allosteric inhibitor that reduces channel gating. This process reduces the apparent affinity of the transduction channel for ligand[36]. Although olfactory transduction is fundamentally different in *Drosophila* from mammals, olfactory adaptation is qualitatively similar: in both cases, adapted responses resemble responses to lower odor concentrations. Similar observations have been reported in moth ORNs[37].

In most sensory systems, adaptation helps to extend the dynamic range of encoding by adjusting the range of neural responses to the current range of stimulus intensities. This idea is consistent with our finding that adaptation in *Drosophila* ORNs represents a negative feedback loop that adjusts the apparent affinity of the receptor for the odor. Because adaptation strongly reduces weak responses but weakly reduces strong responses, it should make ORNs relatively insensitive to small fluctuations in the level of background odor without compromising the ability of ORNs to encode large fluctuations.

The shape of the differentiating spike filter

A recent study has shown that ORN spikes encode both the concentration of an odor stimulus and its rate of change[24]. Our results indicate that sensitivity to the rate of change arises mostly at the level of spiking, rather than transduction. Moreover we found that the same differentiating spike filter described the transformation between input current and spiking in different types of ORN and when the same ORN was presented with different odors.

The shape of this filter explains many of the distinctive features of ORN responses. It can account for why some odors produce transient responses but others do not, and for why inhibitory stimuli produce excitation after odor offset (**Supplementary Fig. 7**). Finally, it helps to explain the results of receptor swap experiments. Namely, if all ORNs impose the same differentiating spiking transformation on their input currents, then receptor swap will recapitulate not only the simpler dynamics of transduction, but also the more complex dynamics of spiking.

ORN spiking dynamics fall on a continuum of behaviors observed in other neurons. Some neurons in the early auditory system behave as nearly pure differentiators[38], whereas cortical pyramidal neurons behave as nearly pure integrators[39]. A Hodgkin-Huxley neuron can produce behaviors that range from differentiation to integration, depending on the Na^+/K^+ conductance ratio[25]. As predicted by this model, we were able to shift the spike response of ORNs from mixed differentiation-integration toward pure differentiation by reducing Na^+ conductance genetically. This result implies that the ORN spike filter is specified by the regulated expression of voltage-dependent conductances and does not require any additional biophysical mechanisms.

Although the shapes of the spike filters we measured were similar across odors and ORNs, we did find that filter size was inversely related to the magnitude of fluctuations in the transduction current. This type of adaptive rescaling occurs in simulated integrate-and-fire neurons simply as consequence of the nonlinearities that are inherent in voltage-dependent conductances[40]. This result is thus consistent with the idea that the spike filter reflects the balance of intrinsic conductances in the cell.

Transduction and spiking shape responses to odor plumes

Consistent with previous findings[1], we found that the time course of odor encounters in a wind-borne plume provided information about the location of the odor source. Here we show that both transduction and spike generation shape the way in which these turbulent stimuli are encoded.

First, we found that transduction lowpass filtered responses to turbulent stimuli with a different time constant for each ligand-receptor pair. ORNs thereby act as a set of temporal filters that collectively analyze an odor filament on many time scales. However, unlike neurons in the auditory system, which are dedicated to encoding information about a specific frequency range, a single ORN encodes temporal information on different time scales depending on the ligand.

Second, we found that the spike transformation increased the speed and sensitivity with which odor fluctuations were encoded. A similar transformation occurs between ORN spike rates and the spike rates of their postsynaptic targets in the brain[41]. This suggests that one function of the ascending olfactory system may be to make neural responses as fast as possible, given the limits of transduction. A similar iterative speeding has been observed in successive layers of the retina[42] and it might be a general feature of many sensory systems.

Comparisons with olfactory dynamics in vertebrates

Our results support the idea that the diverse dynamics of olfactory transduction reflect diverse kinetic rate constants for different receptor-ligand pairs. This concept should generalize to vertebrates, even though vertebrate transduction is mediated by G proteins. Consistent with this idea, recent imaging studies in the rodent olfactory bulb have shown that the time course of ORN activity is ligand-, receptor- and concentration-dependent[43,44].

However, transduction is much slower in vertebrates than in insects. For example, in dissociated frog ORNs, the response to a brief pulse of odor (25 ms) requires about 400 ms to peak and almost 1,000 ms to terminate[45]. By contrast, we found that the fastest responses could peak in <30 ms and terminate in <200 ms (**Fig. 8e**). Our results are consistent with other measurements in *Drosophila*[16] and moths[46].

The difference in speed between vertebrate and insect transduction may reflect the fact that metabotropic signaling is slower than ionotropic signaling.

It is also worth noting that the 'natural temporal statistics' of odors are probably different for different organisms. In terrestrial vertebrates, olfaction is linked to respiration, which imposes a slow oscillation on olfactory signals[44]. Respiration might also tend to enforce laminar flow and disperse odor filaments before odorant receptor binding. By contrast, insect odorant receptors encounter odor filaments more directly. It is tempting to speculate that this difference in the natural temporal statistics of odors might have driven the divergence between ionotropic and metabotropic transduction.

METHODS

Methods and any associated references are available in the online version of the paper at http://www.nature.com/natureneuroscience/.

Note: Supplementary information is available on the Nature Neuroscience website.

ACKNOWLEDGMENTS

We thank J.R. Carlson for Or33c-Gal4, Or46a-Gal4, UAS-Or47a and UAS-Or47b, B.J. Dickson for Or59c-Gal4 and Or42a-Gal4, L. Luo for pebbled-Gal, L. Stevens for UAS-DTl, J.S. Bell, J.B. Cohen, A.L. Fairhall, M. Wachowiak and G. Yellen for conversations, and A.W. Liu, M. Meister, D. Schoppik and members of the Wilson laboratory for feedback on the manuscript. This work was funded by a Helen Hay Whitney Foundation Fellowship (to K.I.N.), a grant from the US National Institutes of Health (R01DC008174), a McKnight Scholar Award and a Beckman Young Investigator Award (to R.I.W.), and a Howard Hughes Medical Institute Early Career Scientist award (to R.I.W.).

AUTHOR CONTRIBUTIONS

K.I.N. performed the experiments and analyzed the data. K.I.N. and R.I.W. designed the experiments and wrote the paper.

COMPETING FINANCIAL INTERESTS

The authors declare no competing financial interests.

Published online at http://www.nature.com/natureneuroscience/.
Reprints and permissions information is available online at http://www.nature.com/reprintsandpermissions/.

1. Murlis, J., Elkinton, J.S. & Cardé, R.T. Odor plumes and how insects use them. *Annu. Rev. Entomol.* **37**, 505–532 (1992).
2. Vickers, N.J., Christensen, T.A., Baker, T.C. & Hildebrand, J.G. Odour-plume dynamics influence the brain's olfactory code. *Nature* **410**, 466–470 (2001).
3. Kang, J. & Caprio, J. Electrophysiological responses of single olfactory bulb neurons to binary mixtures of amino acids in the channel catfish, *Ictalurus punctatus*. *J. Neurophysiol.* **74**, 1435–1443 (1995).
4. de Bruyne, M., Clyne, P.J. & Carlson, J.R. Odor coding in a model olfactory organ: the *Drosophila* maxillary palp. *J. Neurosci.* **19**, 4520–4532 (1999).
5. Reisert, J. & Matthews, H.R. Adaptation of the odour-induced response in frog olfactory receptor cells. *J. Physiol. (Lond.)* **519**, 801–813 (1999).
6. de Bruyne, M., Foster, K. & Carlson, J.R. Odor coding in the *Drosophila* antenna. *Neuron* **30**, 537–552 (2001).
7. Störtkuhl, K.F., Hovemann, B.T. & Carlson, J.R. Olfactory adaptation depends on the Trp Ca^{2+} channel in *Drosophila*. *J. Neurosci.* **19**, 4839–4846 (1999).
8. Gu, Y., Lucas, P. & Rospars, J.P. Computational model of the insect pheromone transduction cascade. *PLOS Comput. Biol.* **5**, e1000321 (2009).
9. Flecke, C. & Stengl, M. Octopamine and tyramine modulate pheromone-sensitive olfactory sensilla of the hawkmoth *Manduca sexta* in a time-dependent manner. *J. Comp. Physiol. A Neuroethol. Sens. Neural Behav. Physiol.* **195**, 529–545 (2009).
10. Kaissling, K.E. Flux detectors versus concentration detectors: two types of chemoreceptors. *Chem. Senses* **23**, 99–111 (1998).
11. Hallem, E.A., Ho, M.G. & Carlson, J.R. The molecular basis of odor coding in the *Drosophila* antenna. *Cell* **117**, 965–979 (2004).
12. Sato, K. *et al.* Insect olfactory receptors are heteromeric ligand-gated ion channels. *Nature* **452**, 1002–1006 (2008).
13. Benton, R., Sachse, S., Michnick, S.W. & Vosshall, L.B. Atypical membrane topology and heteromeric function of *Drosophila* odorant receptors *in vivo*. *PLoS Biol.* **4**, e20 (2006).
14. Yao, C.A. & Carlson, J.R. Role of G proteins in odor-sensing and CO_2-sensing neurons in *Drosophila*. *J. Neurosci.* **30**, 4562–4572 (2010).
15. Wicher, D. *et al.* *Drosophila* odorant receptors are both ligand-gated and cyclic-nucleotide-activated cation channels. *Nature* **452**, 1007–1011 (2008).
16. Schuckel, J., Torkkeli, P.H. & French, A.S. Two interacting olfactory transduction mechanisms have linked polarities and dynamics in *Drosophila melanogaster* antennal basiconic sensilla neurons. *J. Neurophysiol.* **102**, 214–223 (2009).
17. Dobritsa, A.A., van der Goes van Naters, W., Warr, C.G., Steinbrecht, R.A. & Carlson, J.R. Integrating the molecular and cellular basis of odor coding in the *Drosophila* antenna. *Neuron* **37**, 827–841 (2003).
18. Goldman, A.L., van der Goes van Naters, W., Lessing, D., Warr, C.G. & Carlson, J.R. Coexpression of two functional odor receptors in one neuron. *Neuron* **45**, 661–666 (2005).
19. Johnston, D. & Wu, S.M.-S. *Foundations of Cellular Neurophysiology* (MIT Press, 1995).
20. Kaissling, K.E. Chemo-electrical transduction in insect olfactory receptors. *Annu. Rev. Neurosci.* **9**, 121–145 (1986).
21. Schneider, D. Insect olfaction: deciphering system for chemical messages. *Science* **163**, 1031–1037 (1969).
22. Baccus, S.A. & Meister, M. Fast and slow contrast adaptation in retinal circuitry. *Neuron* **36**, 909–919 (2002).
23. Nagel, K.I. & Doupe, A.J. Temporal processing and adaptation in the songbird auditory forebrain. *Neuron* **51**, 845–859 (2006).
24. Kim, A.J., Lazar, A.A. & Slutskiy, Y.B. System identification of *Drosophila* olfactory sensory neurons. *J. Comput. Neurosci.* published online doi:10.1007/s10827-010-0265-0 (21 August 2010).
25. Lundstrom, B.N., Hong, S., Higgs, M.H. & Fairhall, A.L. Two computational regimes of a single-compartment neuron separated by a planar boundary in conductance space. *Neural Comput.* **20**, 1239–1260 (2008).
26. Hallem, E.A. & Carlson, J.R. Coding of odors by a receptor repertoire. *Cell* **125**, 143–160 (2006).
27. Geffen, M.N., Broome, B.M., Laurent, G. & Meister, M. Neural encoding of rapidly fluctuating odors. *Neuron* **61**, 570–586 (2009).
28. Rushton, W.A. Pigments and signals in colour vision. *J. Physiol.* **220**, 1P–P (1972).
29. Laurent, G., Wehr, M. & Davidowitz, H. Temporal representations of odors in an olfactory network. *J. Neurosci.* **16**, 3837–3847 (1996).
30. Daly, K.C., Wright, G.A. & Smith, B.H. Molecular features of odorants systematically influence slow temporal responses across clusters of coordinated antennal lobe units in the moth *Manduca sexta*. *J. Neurophysiol.* **92**, 236–254 (2004).
31. Stopfer, M., Jayaraman, V. & Laurent, G. Intensity versus identity coding in an olfactory system. *Neuron* **39**, 991–1004 (2003).
32. Raman, B., Joseph, J., Tang, J. & Stopfer, M. Temporally diverse firing patterns in olfactory receptor neurons underlie spatiotemporal neural codes for odors. *J. Neurosci.* **30**, 1994–2006 (2010).
33. Soo, F.S., Detwiler, P.B. & Rieke, F. Light adaptation in salamander L-cone photoreceptors. *J. Neurosci.* **28**, 1331–1342 (2008).
34. Deshpande, M., Venkatesh, K., Rodrigues, V. & Hasan, G. The inositol 1,4,5-trisphosphate receptor is required for maintenance of olfactory adaptation in *Drosophila* antennae. *J. Neurobiol.* **43**, 282–288 (2000).
35. Neuhaus, E.M. *et al.* Odorant receptor heterodimerization in the olfactory system of *Drosophila melanogaster*. *Nat. Neurosci.* **8**, 15–17 (2005).
36. Liu, M., Chen, T.Y., Ahamed, B., Li, J. & Yau, K.W. Calcium-calmodulin modulation of the olfactory cyclic nucleotide–gated cation channel. *Science* **266**, 1348–1354 (1994).
37. Kaissling, K.E., Zack Strausfeld, C. & Rumbo, E. Adaptation processes in insect olfactory receptors. Mechanisms and behavioral significance. *Ann. NY Acad. Sci.* **510**, 104–112 (1987).
38. Reyes, A.D., Rubel, E.W. & Spain, W.J. Membrane properties underlying the firing of neurons in the avian cochlear nucleus. *J. Neurosci.* **14**, 5352–5364 (1994).
39. Rauch, A., La Camera, G., Luscher, H.R., Senn, W. & Fusi, S. Neocortical pyramidal cells respond as integrate-and-fire neurons to *in vivo*–like input currents. *J. Neurophysiol.* **90**, 1598–1612 (2003).
40. Famulare, M. & Fairhall, A. Feature selection in simple neurons: how coding depends on spiking dynamics. *Neural Comput.* **22**, 581–598 (2010).
41. Bhandawat, V., Olsen, S.R., Schlief, M.L., Gouwens, N.W. & Wilson, R.I. Sensory processing in the *Drosophila* antennal lobe increases the reliability and separability of ensemble odor representations. *Nat. Neurosci.* **10**, 1474–1482 (2007).
42. Field, G.D., Sampath, A.P. & Rieke, F. Retinal processing near absolute threshold: from behavior to mechanism. *Annu. Rev. Physiol.* **67**, 491–514 (2005).
43. Spors, H., Wachowiak, M., Cohen, L.B. & Friedrich, R.W. Temporal dynamics and latency patterns of receptor neuron input to the olfactory bulb. *J. Neurosci.* **26**, 1247–1259 (2006).
44. Carey, R.M., Verhagen, J.V., Wesson, D.W., Pirez, N. & Wachowiak, M. Temporal structure of receptor neuron input to the olfactory bulb imaged in behaving rats. *J. Neurophysiol.* **101**, 1073–1088 (2009).
45. Bhandawat, V., Reisert, J. & Yau, K.W. Elementary response of olfactory receptor neurons to odorants. *Science* **308**, 1931–1934 (2005).
46. Almaas, T.J., Christensen, T.A. & Mustaparta, H. Chemical communication in heliothine moths. 1. Antennal receptor neurons encode several features of intraspecific and interspecific odorants in the male corn-earworm moth *Helicoverpa zea*. *J. Comp. Physiol. A Neuroethol. Sens. Neural Behav. Physiol.* **169**, 249–258 (1991).

ONLINE METHODS

Fly stocks and genetic strategies. Flies were reared at 25 °C on conventional cornmeal agar medium. All experiments were performed on adult female flies 2–7 days post-eclosion. Stocks are described elsewhere as follows: *Or42a*^{f04305} (ref. 47), *Or85d*$^{-/-}$ (ref. 47), *Or85e*$^{-/-}$ (ref. 47), *pebbled-Gal4* (ref. 48), *UAS-DTl* (L.M. Stevens, http://flybase.org/; personal communication to FlyBase FBrf0204962), *Or33c-Gal4* (ref. 18), *Or46a-Gal4* (ref. 18), *Or59c-Gal4* (ref. 49), *UAS-DmNa$_v$-IR* (Vienna *Drosophila* RNAi Center, http://stockcenter.vdrc.at/, stocks 6131 and 6132), *Or42a-Gal4* (ref. 49), *UAS-OR47a* (ref. 17) and *UAS-OR47b* (ref. 11). We used the following genotypes to produce flies with one active neuron in a sensillum, and to verify that LFP responses from this sensillum type were due to a single type of OR.

Sensillum pb1: to record from pb1A, we primarily used a strain (*w*^{1118}) in which the pb1B neuron is silent because this strain likely harbors a mutation in *Or71a* (ref. 18). (Some pilot recordings were performed in the genotype *NP3481-Gal4;UAS-CD8:GFP*, in which pb1B is functional; we found that pb1 recordings in this genotype were not different from those in *w*^{1118}, because pb1B is narrowly selective for an odor that we did not use.) To silence pb1A, we used a mutation in *Or42a* (*Or42a*^{f04305}). Some pilot experiments were performed in the genotype *Or42a*^{f04305}; *TM3/TM6b*; here, TM3 supplies a functional copy of *Or71a* (ref. 18), which was useful for identifying the pb1 sensillum (data not shown).

Sensillum pb2: to record from pb2A, we killed pb2B by expressing diphtheria toxin light chain under Gal4/UAS control (*Or46a-Gal4/UAS-DTl;UAS-DTl/+*). To record from pb2B, we killed pb2A (*Or33c-Gal4/UAS-DTl;UAS-DTl/+*). To silence both pb2 neurons, we killed them both (*Or46a-Gal4/Or33c-Gal4;UAS-DTl/+*), or we killed pb2B and silenced pb2A by mutating *Or85e* (*Or46a-Gal4/UAS-DTl;Or85e*$^{-/-}$).

Sensillum pb3: to record from pb3B, we killed pb3A (*Or59c-Gal4/+,UAS-DTl/+;UAS-DTl/+*). To silence both pb3 neurons, we killed pb3A and silenced pb3B by mutating *Or85d* (*Or59c-Gal4/+;UAS-DTl/+;Or85d*$^{-/-}$).

The lines designated *Or85d*$^{-/-}$ and *Or85e*$^{-/-}$ in this study represent the same genotype, which is called *Δ85* in ref. 47. This mutation abolishes odor responses in both pb2A and pb3B, and probably represents a genetic lesion that eliminates both of these receptors.

To knock down Na^+ channel expression in ORNs, we used flies of the following genotype: *pebbled-Gal4/+;UAS-DmNa$_v$-IR/+*. Control flies lacked the inverted-repeat transgene (*pebbled-Gal4/+;TM3/+*). The two *UAS-DmNa$_v$-IR* stocks produced similar results, and so data from the two genotypes were combined.

Self-adaptation experiments in **Figure 6c**,**d** and cross-adaptation experiments in **Figure 7a**,**b** were performed in the same genotype (*Or42a-Gal4/+;UAS-Or47a/+*). Similar results for self-adaptation were obtained in two control genotypes (*w*^{1118} and *pebbled-Gal4*, data not shown). Cross-adaptation experiments in **Figure 7c**,**d** were performed in the genotype *UAS-Or47b/+;Or42-Gal4/+*. Control experiments to verify that each cross-adaptation stimulus was specific to just one of the two odorant receptors are described in **Supplementary Fig. 5**. The self-adaptation experiment used a higher concentration of 2-butanone than any of our other experiments (0.2×), so we also did additional control experiments to verify that this stimulus produced very little LFP deflection in *Or42a* mutants (genotype *Or42a*^{f04305}, mean LFP response, −0.5 5 ± 0.30 mV). Spontaneous firing rates in pb1A neurons misexpressing OR47b (*UAS-Or47b/+;Or42-Gal4/+*) were significantly higher than spontaneous firing rates in normal pb1A neurons (*Or42a-Gal4/CyO*, $P < 0.01$) or pb1A neurons misexpressing OR47a (*Or42a-Gal4/+;UAS-Or47a/+*, $P < 0.01$). The comparison of spontaneous firing rates and initial response amplitudes to 2-butanone in pb1A neurons in the text refers to a comparison between *UAS-Or47b/+;Or42-Gal4/+* and *Or42a-Gal4/+;UAS-Or47a/+*.

Electrophysiology. The fly was cold-anesthetized and wedged into the tip of a modified plastic pipette with the body, head, and proboscis waxed into place. The fly was then fixed under an upright compound microscope with a 50× air objective (Olympus BX51). The palp was stabilized between a glass pipette and a glass coverslip. A reference electrode filled with saline was placed in the eye and a silver chloride electrode inside a saline-filled sharp glass micropipette was inserted into the sensillum lymph.

Within the sensillum lymph, the resting potential was higher than within the surrounding hemolymph[20], and odor-induced LFPs were larger, presumably because the path between recording and reference electrodes has higher resistance within than outside the sensillum. Spike waveforms recorded inside the sensillum had the shape characteristic of extracellular recordings, indicating that our electrodes did not penetrate ORN dendrites. Sensillum types were identified by their characteristic responses to a panel of odors[4] or as described in the text. Electrical signals were acquired using a Model 2400 amplifier (A-M Systems) and lowpass filtered at 2 kHz with a LPF202A signal conditioner (Warner Instruments) before digitization at 10 kHz. Where filters for multiple odors were calculated for the same neuron type, each recorded individual neuron was generally tested with all these odors.

Spikes were identified using custom routines written in MATLAB that filtered, differentiated and thresholded the raw signal. For pb1 and ab5 recordings, the two spike types were easily identified on the basis of spike size. For the other sensilla, we recorded from flies in which one neuron was killed so only a single spike type remained. LFP signals were extracted from the raw trace by lowpass filtering at 15 Hz with a digital 2-pole Butterworth filter implemented in MATLAB. Spike times and LFPs were down-sampled to 1 kHz for display and analysis. For the experiments in **Figure 2** using TTX, the drug was dissolved in saline (50 μM) and injected into the body of the palp using a syringe-driven glass micropipette. After 2–3 pulses of pressure we saw the injected liquid move into the palp. Recordings started 5 min after injection. TTX and saline injections were randomly interleaved and in most experiments the experimenter was blind to the contents of the injection. Post-hoc analysis revealed that spiking was completely abolished after all TTX injections and no saline injections.

Note that all recordings (except for ab5 and trichoid recordings shown in **Supplementary Fig. 5**) were performed from palp sensilla. This is because sensilla are less densely packed on the palp than on the antenna, which permits better isolation of LFP signals arising from single sensilla. However, the time course of ORN spiking responses was not systematically different in antennal from in palp sensilla (data not shown). Thus, our major conclusions are likely to generalize to these ORNs as well.

Odor delivery. In **Figures 1**–**7**, odors were delivered using a custom-built device designed to allow stable and repeated presentation of long-duration odor stimuli (**Supplementary Fig. 1**). The design of this device means that odors were delivered at an effective concentration that is substantially lower than what would be delivered using a more conventional device and the same nominal odor dilutions in solvent. A 1-mL vial was filled with 900 μL of pure odorant or odorant diluted in paraffin oil (J.T. Baker, VWR #JTS894). A continuous stream of air (100 ml min^{-1}) passed over the vial and was diluted in a second air stream (100 ml min^{-1}) before venting into a vacuum tube. To allow the head space of the vial to equilibrate with the air flowing over it, an odor vial was placed in the device at least 20 min before odor was first delivered to the fly, during which time the odor concentration in the air stream reached a steady state (**Supplementary Fig. 1**). For experiments in which several odors were presented briefly (test pulse odors in **Figs. 6** and **7** and control experiments to verify the privacy of these odors in **Supplementary Fig. 5**), odor vials were placed in the device for only 5 min before presentation. In general, experiments using a single odor were completed before switching to a different odor. During an experiment, a three-way solenoid valve allowed us to rapidly switch the odor stream from the vacuum tube into a delivery air stream (1 l min^{-1}) directed at the fly. The air flow rates in the vacuum and delivery tubes were equalized to minimize transients during switching. In some of the LFP traces shown, a brief electrical artifact caused by the solenoid was deleted for display purposes and the trace was mended by linear extrapolation between the cut ends; the maximum time blanked was 200 ms. Adaptation experiments (**Figs. 6** and **7**) were performed using a modified olfactometer with two parallel sets of valves, mixing tubes, and odor vials. We used a photoionization detector to verify that each channel could deliver odor independently.

In **Figure 8**, an open vial of odor was placed 5–35 cm downwind of a small fan (Rosewill DFS802512M or Caframo Tiny Tornado 827 BL) and upwind of the fly (or PID). The windspeed at the fly was measured using a hot wire anemometer (Kanomax A004) and ranged from 0.11 to 0.39 m s^{-1}. This is within the range of wind speeds encountered by *Drosophila* in its native habitat, according to a study that measured a mean of 0.37 m s^{-1} and a range of ±0.35 m s^{-1} in an orange orchard where *Drosophila* were active[50]. To vary crosswind distance (x), the vial was moved perpendicular to the line connecting the fan and the fly. To vary upwind distance (y), the fly was moved away from the vial along this line.

When the odor vial was removed, LFP events disappeared and only spontaneous spikes remained.

Data analysis. Peristimulus time histograms (PSTHs) were calculated by taking the mean spike train across trials, then convolving spike times with a 50-ms Hanning window. Spontaneous firing rates were calculated over the 4 s preceding stimulus presentation. In **Figure 2**, mean LFP amplitude was computed over a 1,200-ms window beginning 300 ms after stimulus onset and ending 500 ms after offset. In **Figure 5c**, we fit an exponential function with a variable decay rate and variable steady-state value to each PSTH, beginning from its peak and ending 200 ms after nominal only stimulus offset (valve closing). In **Figure 5d**, we calculated the peak-to-steady-state ratio by comparing the maximum of each PSTH to the mean firing rate over a 400-ms period beginning 800 ms after nominal stimulus onset (valve opening). In **Figure 6b**, on and off rates were computed by fitting an exponential function with a variable decay rate and latency to the normalized mean LFP. To compute on rates, we fit a 1-s period from nominal stimulus onset to offset. To compute off rates, we fit the remainder of the trial (10 s) beginning at nominal stimulus offset. Mean response amplitudes in **Figures 6e** and **7a–c** were calculated over a 400-ms period starting 300 ms after nominal stimulus onset. For **Figure 7d**, mean response amplitude was calculated over 1,300 ms. Onset rates for **Figures 6f** and **7a–c** were calculated by fitting an exponential function as in **Figure 6b**, but for the 500-ms period from nominal stimulus onset to offset. In **Figure 8e**, we detected discrete events in the LFP by lowpass filtering the raw voltage trace at 15 Hz, differentiating, and looking for threshold crossings in the resulting signal. Events were binned by peak amplitude in bins of 4 mV over the range 2–26 mV. Compound events were identified by having values above 10 mV during a window 50 ms before or 300 ms after initiation, and were eliminated from the analysis. In **Figure 8g**, peak spike rate was computed over 30 ms preceding the LFP peak.

Filter analysis. To estimate linear filters, we delivered odor with a slowly varying, random time course. The time course was created from binary random values sampled at 20 Hz, passed through an exponential lowpass filter with a time constant of 3 s, then rounded to obtain a binary signal. We used offline simulations to verify that this stimulus could be used to correctly estimate the shape of a linear filter. LFPs and spike times were further down-sampled to 100 Hz for filter analysis.

In general, the linear filter that transforms an input I into a response R can be calculated in the frequency domain according to

$$F(\omega) = \frac{I^*(\omega)R(\omega)}{I^*(\omega)I(\omega)}$$

where $F(\omega)$, $I(\omega)$ and $R(\omega)$ are the Fourier transforms of the filter, input and response, respectively. The variable ω represents frequency and the asterisk represents the complex conjugate. The numerator of this equation is equal to the Fourier transform of the cross-correlogram of input and response:

$$C(\tau) = \int dt R(t)I(t-\tau)$$

and the denominator is the power spectrum of the input.

For all the filters we calculated, both the input and output signals had relatively little high-frequency content, and so the filter was poorly estimated at high frequencies. Moreover, because the input signal had little power at high frequencies, normalizing by the power spectrum of the input signal tended to boost this high-frequency noise in the filter. Therefore, to obtain a reasonable filter, we gradually attenuated the frequency representation of the filter above a cutoff frequency (f_{cut}) according to

$$c(\omega) = e^{-\frac{|\omega - f_{cut}|}{f_\tau}} \quad \text{for } |\omega| \geq f_{cut}$$

before transforming it back into the time domain. Gradual attenuation was used to reduce ripples in the filter that arise from a sharp frequency cutoff. For odor-to-LFP filters we chose $f_{cut} = 5$ Hz, $f_\tau = 20$ Hz and for LFP-to-spike rate filters we chose $f_{cut} = 5$ Hz, $f_\tau = 200$ Hz. For filters relating the theoretical command signal to the PID response we used $f_{cut} = 10$ Hz, $f_\tau = 50$ Hz. In general, we chose the largest values of f_{cut} and f_τ that did not introduce excessive noise into the resulting filter. Qualitatively similar results were obtained with higher absolute cutoffs and sharper attenuation, though this produced more ripples at the edges of the filter.

In general, the power spectrum of the input signal limits the power spectrum of the calculated filter. In our case, the fact that the LFP had little power at high frequencies means that the calculated spike filter could not contain high frequencies. The true spike filter is almost certainly quite narrow, and so the calculated spike filter is probably a smoothed version of the true spike filter (**Supplementary Fig. 3**). This smoothing is what causes the calculated spike filter to have some structure to the right of the zero time point. In addition, the calculated spike filter may include a small contribution from the spike waveform itself.

Data used to test the filter were kept separate from data used to calculate the filter. MATLAB (MathWorks) was used to produce stimulus waveforms, analyze the data and perform simulations.

47. Olsen, S.R., Bhandawat, V. & Wilson, R.I. Excitatory interactions between olfactory processing channels in the *Drosophila* antennal lobe. *Neuron* **54**, 89–103 (2007).
48. Sweeney, L.B. *et al.* Temporal target restriction of olfactory receptor neurons by Semaphorin-1a/PlexinA-mediated axon-axon interactions. *Neuron* **53**, 185–200 (2007).
49. Couto, A., Alenius, M. & Dickson, B.J. Molecular, anatomical, and functional organization of the *Drosophila* olfactory system. *Curr. Biol.* **15**, 1535–1547 (2005).
50. Budick, S.A. & Dickinson, M.H. Free-flight responses of *Drosophila melanogaster* to attractive odors. *J. Exp. Biol.* **209**, 3001–3017 (2006).

doi:10.1038/nn.2725